Local accumulation times in a diffusion-trapping model of receptor dynamics at proximal axodendritic synapses

Ryan D. Schumm and P. C. Bressloff

Department of Mathematics, University of Utah, 155 South 1400 East, Salt Lake City, Utah 84112, USA

The lateral diffusion and trapping of neurotransmitter receptors within the postsynaptic membrane of a neuron play a key role in determining synaptic strength and plasticity. Trapping is mediated by the reversible binding of receptors to scaffolding proteins (slots) within a synapse. In this paper we introduce a method for analyzing the transient dynamics of proximal axodendritic synapses in a diffusion-trapping model of receptor trafficking. Given a population of spatially distributed synapses, each of which has a fixed number of slots, we calculate the rate of relaxation to the steady-state distribution of bound slots (synaptic weights) in terms of a set of local accumulation times. Assuming that the rates of exocytosis and endocytosis are sufficiently slow, we show that the steady-state synaptic weights are independent of each other (purely local). On the other hand, the local accumulation time of a given synapse depends on the number of slots and the spatial location of all the synapses, indicating a form of transient heterosynaptic plasticity. This suggests that local accumulation time measurements could provide useful information regarding the distribution of synaptic weights within a dendrite.

I. INTRODUCTION

The lateral diffusion and trapping of neurotransmitter receptors within the postsynaptic membrane of a neuron plays a key role in mediating synaptic strength and plasticity [1–16]. The two most studied examples are glycine receptors (GlyRs) and α-amino-3-hydroxy-5-methyl-4-isoxazole-propionic acid receptors (AMPARs), although diffusion trapping appears to be a general mechanism for most types of neurotransmitter receptors. GlyRs are ligand-gated ion channels that mediate chloride-dependent synaptic inhibition and are found in the postsynaptic membrane of the soma and initial portion of dendrites in spinal cord neurons. Single particle tracking (SPT) experiments have shown that GlyRs alternate between diffusive and confined states at the cell surface, and confinement is spatially associated with postsynaptic densities (PSDs) that contain the scaffolding protein gephyrin [1,3]. The majority of fast excitatory synaptic transmission in the central nervous system is mediated by the neurotransmitter glutamate binding to AMPARs located in the postsynaptic membrane of dendritic spines. Again SPT experiments reveal that AMPARs diffuse freely within the dendritic membrane until they enter a spine, where they are temporarily confined by the geometry of the spine and through interactions with scaffolding proteins such as PSD-95 and cytoskeletal elements within the PSD [2,6]. A surface receptor in either type of synapse may also be internalized via endocytosis and stored within an intracellular compartment, where it is either recycled to the surface via recycling endosomes and exocytosis or sorted for degradation by late endosomes and lysosomes [17].

A number of models have explored the combined effects of diffusion trapping and recycling on the number of synaptic AMPARs within dendritic spines [18–23]. In such models, the synapse is treated as a self-organizing compartment in which the number of receptors is a dynamic steady state that determines the strength of the synapse; activity-dependent changes in the strength of the synapse then correspond to shifts in the dynamical set point. Most diffusion-trapping models assume that the number of trapping sites or "slots" within a given synapse is fixed. However, it is known that scaffolding proteins and other synaptic components are also transported into and out of a synapse, albeit at slower rates [24]. Several experimental and modeling studies have analyzed the joint localization of gephyrin scaffolding proteins and GlyRs at synapses [25–29], showing how stable receptor-scaffold domains could arise dynamically.

In this paper we analyze a diffusion-trapping model of receptor trafficking in the case of a population of spatially distributed axodendritic synapses that are proximal to the soma and that have a fixed number of slots. We use the model to investigate how the spatial locations of the synapses and the distribution of slot proteins affect (i) the steady-state number of bound receptors in each synapse (synaptic weights) and (ii) the approach to steady state as determined by a set of local accumulation times. The latter provide a method for characterizing the transient response of synapses. Accumulation times were originally used to estimate the time to form a protein concentration gradient during morphogenesis [30–32]. More recently, they have been applied to a wider range of diffusion processes, including intracellular protein gradient formation [33], search processes with stochastic resetting [34], and gap junctions [35]. The underlying idea is to treat the fractional deviation from the steady-state concentration as a cumulative distribution whose mean is identified with the local accumulation time. One can thus take into account the fact that different spatial regions can relax at different rates.

(This contrasts with a global measure of the relaxation rate based on the principal nonzero eigenvalue of the Laplacian.) In addition, for linear diffusion problems, the accumulation times can be calculated by solving the diffusion equation in Laplace space, which avoids the difficulty in obtaining the full time-dependent solution by evaluating the inverse Laplace transform [36].

In order to introduce the basic approach, we focus on a simplified one-dimensional (1D) model of a dendritic cable, in which the synapses are represented as point sources or sinks at different spatial locations along the cable. We previously showed that reducing two-dimensional (2D) lateral diffusion in the dendritic membrane to 1D diffusion is a reasonable approximation given the large aspect ratio of dendrites [37]. The model does ignore the detailed microstructure of a synapse and the effects of a confining geometry such as the bottleneck of a dendritic spine. However, the latter is not an issue in the case of inhibitory synapses. We first derive a set of reaction-diffusion (RD) equations for the extrasynaptic receptor concentration and the fraction of bound slot proteins in each synapse (Sec. II). We then calculate the steady-state distributions of extrasynaptic and synaptic receptor concentrations by solving the steady-state RD system in terms of the 1D Green's function of the modified Helmholtz equation along lines analogous to Refs. [18,20,21] (Sec. III). Finally, we extend the analysis to calculate the corresponding accumulation times by solving the time-dependent RD equations in Laplace space (Sec. IV). In this case, it is necessary to linearize the equations by assuming that the slot proteins are unsaturated. This is then compared with the more realistic saturated regime using numerical simulations.

For the sake of illustration, we focus in this paper on simple configurations of synapses or synaptic clusters, which are treated as identical, modulo their spatial locations and individual slot protein numbers. (A more realistic model would need to take into account the considerable heterogeneity in synaptic properties, although one could consider some form of homogenized version that is more consistent with our simplified model.) We also interpret the number of bound receptors as the effective synaptic weight or strength. (There is a long-standing debate concerning whether or not synaptic strength is predominately postsynaptic (e.g., number of bound receptors) or presynaptic (e.g., vesicular release probabilities) [4,5,7]. We assume the former here.) Given our various assumptions, we obtain the following results. First, for a cluster of closely spaced synapses, the steady-state fraction of bound receptors in each synapse is the same. This implies that an increase in the rate of slot binding under some form of long term potentiation, say, scales all synaptic strengths by the same factor (multiplicative scaling). An analogous result was previously found in a nonspatial, compartmental model [23]. However, multiplicative scaling breaks down for spatially separated synapses and when synapses are located sufficiently close to the soma. We then show that, in contrast to the synaptic weights, the local accumulation times depend on the distribution of slot proteins across all the synapses. For both the steady-state solution and accumulation times, we demonstrate that two different modes of behavior can be observed, corresponding to small and large exocytosis rates, respectively.
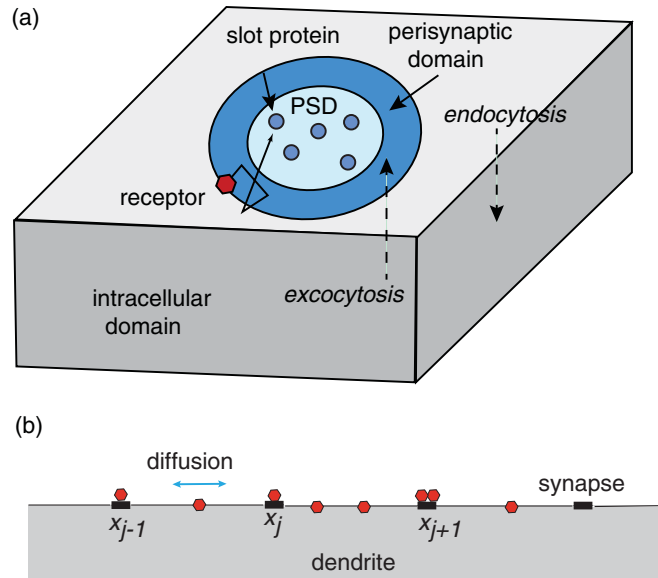

FIG. 1. (a) Schematic illustration of a diffusion-trapping model for a protein receptor by a single inhibitory synapse. The receptor diffuses freely extrasynaptically but can transiently bind to scaffolding protein slots within the PSD. The PSD thus acts as a trapping region. Receptors can also be inserted into or removed from the surface via exocytosis or endocytosis. (b) Schematic illustration of the 1D diffusion-trapping model. Each synapse is treated as a point source or sink for receptors that diffuse along a 1D dendritic cable.

II. DIFFUSION-TRAPPING MODEL

In Fig. 1(a) we show a simplified schematic diagram of a single inhibitory synapse in the plasma membrane of a neuron. A neurotransmitter receptor diffuses freely in the extrasynaptic membrane, which means that its mean-square displacement is proportional to Dt, where t is the elapsed time in the free state and D is the membrane diffusivity. However, on entering the PSD it can reversibly bind to a scaffolding or slot protein, which has the effect of temporarily confining or trapping the receptor within the PSD. This can be amplified by molecular crowding within the PSD, which slows the rate of diffusion, and by geometrical factors such as the narrow neck of a dendritic spine in the case of an excitatory synapse [38–41]. Recent imaging studies of the microstructure of the PSD suggest that there exist PSD microdomains containing higher densities of scaffolding proteins, where most of the receptors are stabilized [42,43]; outside of these domains, receptors tend to diffuse more freely. For simplicity, we ignore the detailed microstructure of a PSD by treating the PSD as a homogeneous medium within which a receptor can bind at a rate that is proportional to the number of slots. We also allow for receptors to be transferred from the surface membrane to intracellular compartments via an internalization process known as endocytosis [17]. Intracellular receptors can also be inserted into the membrane via exocytosis. Experimentally, it has been found that sites of exocytosis and endocytosis exist within the proximity of synapses as well as various extrasynaptic locations. In our model, we assume that endocytosis occurs everywhere, whereas exocytosis occurs (peri)synaptically. However, one could modify these assumptions accordingly.

Following Refs. [18,20,21], we treat the domain Ω as a 1D dendritic cable in which the synapses are represented as point sources or sinks on the cable [see Fig. 1(b)]. This particular approach exploits the fact that the length of a dendrite is typically several hundred microns, which is at least two orders of magnitude greater than the radius of a dendrite and the size of a synapse. Additionally, we are leveraging the fact that the Green's function of the 1D diffusion equation is nonsingular (in contrast to higher spatial dimensions) so that we avoid introducing singular solutions when modeling the dendritic spines as point-like sources or sinks [37].

Suppose that Ω is a semi-infinite cable with the axial coordinate $x \in [0, \infty)$; $x = 0$ denotes the location of the somatic end of the cable. (Alternatively, we could consider a cable of length L and simply ignore the effects of the distal boundary for sufficiently large L.) Let x_j, $j = 1, \ldots, N$, denote the position of the jth spine. The positions are ordered such that $x_j < x_{j+1}$ for all $j = 1, \ldots, N - 1$. Finally, let $u(x, t)$ denote the concentration of receptors per unit length of cable and S_k and $r_k(t)$ be the number of binding sites and fraction of bound sites in synapse k, respectively. This RD system is then defined according to the following system of equations:

$$\frac{\partial u}{\partial t} = D\frac{\partial^2 u}{\partial x^2} - \gamma u(x, t) + \sum_{k=1}^{N}[S_k g_k(t)$$
$$+ \sigma - \widehat{\gamma} u(x_k, t)]\delta(x - x_k), \tag{2.1a}$$

$$\frac{dr_k}{dt} = \kappa_+ u(x_k, t)[1 - r_k(t)] - \kappa_- r_k(t) \equiv -g_k(t), \tag{2.1b}$$

together with the boundary condition $-D\partial_x u(0, t) = J_0 > 0$. The latter represents a constant flux of receptors injected from the soma. The first term on the right-hand side of Eq. (2.1a) represents the lateral diffusion of receptors in the dendritic membrane with diffusivity D, whereas the second term represents endocytosis of the extrasynaptic receptors at a uniform rate γ. The sum over k takes into account the additional sources of freely diffusing receptors within the N point-like synapses; the latter are represented by the Dirac delta functions $\delta(x - x_k)$, $k = 1, \ldots, N$. The total current in the kth synapse consists of the sum of three terms: σ is the exocytosis current into the perisynaptic domain, $\widehat{\gamma} u(x_k, t)$ is the current due to the endocytosis of unbound synaptic receptors, and $S_k g_k(t)$ is the difference between the unbinding and binding rates associated with the S_k slot proteins. The fractional rate $g_k(t)$ [see Eq. (2.1b)] is the difference between the total unbinding rate $\kappa_- r_k(t)$ and the total binding rate $\kappa_+ u(x_k, t)[1 - r_k(t)]$. The factor $[1 - r_k(t)]$ represents the fraction of unbound slot proteins at time t. Finally, we impose the initial conditions

$$u(x, 0) = 0, \quad r(0) = 0. \tag{2.2}$$

It is important to note that γ, σ, and κ_- have units of inverse time, whereas $\widehat{\gamma}$ and κ_+ have units of speed. Unfortunately, only a few model parameters are known explicitly [23]. These include the unbinding rate $\kappa_- \sim 2.5 \times 10^{-2}$ s^{-1} [44], the rate of internalization $\gamma \sim 10^{-3} - 10^{-2}$ s^{-1} [10], and the membrane diffusivity $D \sim 0.1$ μm^2 s^{-1} [10]. One general observation, however, is that the basal rates of receptor binding and unbinding are at least an order of magnitude faster

than the rates of receptor internalization and externalization, that is, $\kappa_\pm \gg \gamma$.

In this paper we are interested in calculating the steady-state solution of Eqs. (2.1) and the corresponding approach to steady state. We will investigate the latter in terms of the accumulation times of the RD process. In order to construct the accumulation time of $u(x, t)$ to reach the steady-state $u^*(x)$, consider the function

$$Z(x, t) = 1 - \frac{u(x, t)}{u^*(x)}, \tag{2.3}$$

which represents the fractional deviation of the concentration from the steady state. Assuming that there is no overshooting, $1 - Z(x, t)$ is the fraction of the exterior steady-state concentration that has accumulated at x by time t. It follows that $-\partial_t Z(x, t)dt$ is the fraction accumulated in the interval $[t, t + dt]$. The accumulation time is then defined as [30–32]

$$T(x) = \int_0^\infty t\left(-\frac{\partial Z(x, t)}{\partial t}\right)dt = \int_0^\infty Z(x, t)dt. \tag{2.4}$$

Finally, by analogy, we can also define an accumulation time for the fraction of bound receptors, namely,

$$\tau_k = \int_0^\infty z_k(t)dt, \quad z_k(t) = 1 - \frac{r_k(t)}{r_k^*}. \tag{2.5}$$

It is often more useful to calculate an accumulation time in Laplace space. First, consider $Z(x, t)$ in Eq. (2.3). Using the identity

$$u^*(x) = \lim_{t \to \infty} u(x, t) = \lim_{s \to 0} s\widetilde{u}(x, s)$$

and setting $\widetilde{F}(x, s) = s\widetilde{u}(x, s)$ imply that

$$s\widetilde{Z}(x, s) = 1 - \frac{\widetilde{F}(x, s)}{\widetilde{F}(x, 0)}$$

and

$$T(x) = \lim_{s \to 0} \widetilde{Z}(x, s) = \lim_{s \to 0} \frac{1}{s}\left[1 - \frac{\widetilde{F}(x, s)}{\widetilde{F}(\mathbf{x}, 0)}\right]$$
$$= -\frac{1}{\widetilde{F}(x, 0)}\frac{d}{ds}\widetilde{F}(x, s)\bigg|_{s=0}. \tag{2.6}$$

Similarly, setting $\widetilde{f}_k(s) = s\widetilde{r}_k(s)$, we have

$$\tau_k = -\frac{1}{\widetilde{f}_k(0)}\frac{d}{ds}\widetilde{f}_k(s)\bigg|_{s=0}. \tag{2.7}$$

III. STEADY-STATE SOLUTION

At steady state we have $g_k(t) = 0$ for all $k = 1, \ldots, N$. Hence, the steady-state equations take the form

$$D\frac{d^2 u^*(x)}{dx^2} - \gamma u^*(x) = -\sum_{k=1}^{N}[\sigma - \widehat{\gamma} u^*(x_k)]\delta(x - x_k), \tag{3.1a}$$

$$r_k^* = \frac{\kappa_+ u^*(x_k)}{\kappa_- + \kappa_+ u^*(x_k)}, \tag{3.1b}$$

and $du^*/dx = -J_0/D$ at $x = 0$. Equation (3.1a) can be solved in terms of the 1D Neumann Green's function $G(x, \xi)$ on

$[0, \infty)$, which is the solution to the equation

$$D\frac{d^2 G(x,\xi)}{dx^2} - \gamma G(x,\xi) = -\delta(x-\xi), \quad \frac{dG(x,\xi)}{dx}\bigg|_{x=0} = 0, \quad (3.2)$$

with $G(x,\xi) \to 0$ as $|x| \to \infty$. One finds that

$$G(x,\xi) = \frac{1}{2\sqrt{D\gamma}}[e^{-\sqrt{\gamma/D}|x-\xi|} + e^{-\sqrt{\gamma/D}(x+\xi)}]. \quad (3.3)$$

It follows that the dendritic surface receptor concentration has an implicit solution of the form

$$u^*(x) = J_0 G(x,0) + \sum_{k=1}^{N} [\sigma - \widehat{\gamma} u^*(x_k)]G(x,x_k). \quad (3.4)$$

The first term represents the effect of the flux at the somatic end $x = 0$.

We can now generate a closed set of equations for the synaptic concentrations $u_j^* = u^*(x_j)$, $j = 1, \ldots, N$, by setting $x = x_j$ in Eq. (3.4):

$$u_j^* = J_0 G(x_j, 0) + \sum_{k=1}^{N} G(x_j, x_k)[\sigma - \widehat{\gamma} u_k^*]. \quad (3.5)$$

This can be rewritten as the matrix equation

$$\sum_{k=1}^{N} \left[\delta_{j,k} + \frac{\widehat{\gamma}}{\sqrt{\gamma D}} \mathcal{G}_{jk} \right] u_k^* = \mathbf{H}_j, \quad (3.6a)$$

with

$$\mathcal{G}_{jk} = \sqrt{\gamma D} G(x_j, x_k), \quad (3.6b)$$

$$\mathbf{H}_j = J_0 G(x_j, 0) + \sigma \sum_{k=1}^{N} G(x_j, x_k). \quad (3.6c)$$

A solution for u_k^*, $k = 1, \ldots, N$, will exist provided that the matrix $\mathbf{I} + \frac{\widehat{\gamma}}{\sqrt{\gamma D}} \mathcal{G}$ is invertible. One way to invert the matrix is to exploit the fact that the rate of endocytosis within a synapse is relatively small (possibly due to receptor clustering and molecular crowding). Therefore, since $G(x, x') \sim 1/\sqrt{D\gamma}$, we assume that

$$\frac{\widehat{\gamma}}{\sqrt{D\gamma}} = \epsilon \gamma_0 \ll 1, \quad (3.7)$$

where γ_0 is a dimensionless $O(1)$ parameter. We can now carry out a perturbation expansion of the steady-state solution (3.5) with respect to ϵ. That is, we write

$$(\mathbf{I} + \epsilon \gamma_0 \mathcal{G})^{-1} = \mathbf{I} - \epsilon \gamma_0 \mathcal{G} + \epsilon^2 \gamma_0^2 \mathcal{G}^2 + \cdots \quad (3.8)$$

and introduce the series expansion

$$u_j^* = u_{j,0}^* + \epsilon u_{j,1}^* + \epsilon^2 u_{j,2}^* + \cdots. \quad (3.9)$$

Substituting Eqs. (3.8) and (3.9) into Eq. (3.5) gives

$$u_{j,0}^* + \epsilon u_{j,1}^* + \epsilon^2 u_{j,2}^* + \cdots$$

$$= \sum_{k=1}^{N} [\delta_{j,k} - \epsilon \gamma_0 \mathcal{G}_{jk} + \epsilon^2 \gamma_0^2 [\mathcal{G}^2]_{jk} + \cdots]$$

$$\times \left[J_0 G(x_k, 0) + \sigma \sum_{l=1}^{N} G(x_k, x_l) \right]. \quad (3.10)$$

Hence, collecting terms in powers of ϵ leads to a hierarchy of equations, the first few of which are as follows:

$$u_{j,0}^* = J_0 G(x_j, 0) + \sigma \sum_{l=1}^{N} G(x_j, x_l), \quad (3.11a)$$

$$u_{j,1}^* = -\gamma_0 \sum_{k=1}^{N} \mathcal{G}_{jk} u_{k,0}^*. \quad (3.11b)$$

The leading order term $u_{j,0}^*$ has two distinct contributions. The first, $J_0 G(x_j, 0)$, represents the exponential-like decay of the flux strength with respect to the spatial distance of the jth synapse from the soma. The second, $\sigma \sum_{l=1}^{N} G(x_j, x_l)$, is a pairwise synaptic interaction term. Clearly, the former contribution will dominate at proximal locations and relatively large flux amplitudes J_0. On the other hand, the latter contribution will dominate at more distal locations, particularly when there are a large number of synapses in a cluster. Finally, substituting the series expansion of u_j^* into Eq. (3.4) shows that $u^*(x) = u_0^*(x) + O(\epsilon)$, with

$$u_0^*(x) = J_0 G(x,0) + \sigma \sum_{k=1}^{N} G(x, x_k). \quad (3.12)$$

Note that $u_{j,0}^* = u_0^*(x_j)$. In Fig. 2, we plot Eq. (3.12) and a numerical steady-state solution obtained by numerically inverting the matrix equation (3.6) for u_k^* and substituting the result into Eq. (3.4). We find that for ϵ values in the range $[0.001, 0.1]$, Eq. (3.12) yields an accurate approximation of the steady-state solution.

If the synapses are clustered in an interval of length $[X, X + \ell]$ with $\ell \ll \sqrt{D/\gamma}$, then $G(x_j, 0) \approx G(X, 0)$, and $G(x_k, x_l) \approx G(X, X)$, so that

$$u_{j,0}^* \approx U(X) \equiv J_0 G(X, 0) + \sigma N G(X, X) \quad (3.13)$$

and

$$r_j^* \approx R(X) \equiv \frac{\kappa_+ U(X)}{\kappa_- + \kappa_+ U(X)} \quad (3.14)$$

for all $j = 1, \ldots, N$, where N is the number of synapses in the cluster. We thus find that the fraction of filled slots in each synapse is the same, irrespective of the number of slot proteins. Suppose that $w_j = S_j r_j^*$ is identified as the steady-state strength of the jth synapse. (For simplicity, we ignore presynaptic factors.) This implies that the ratio of synaptic strengths of any two synapses within the cluster is equal to the ratio of their number of slots. Moreover, if $R(X)$ is modified due to changes in the binding rate κ_+, say, then all synaptic strengths are scaled by the same factor (multiplicative scaling). An analogous result was previously obtained in a
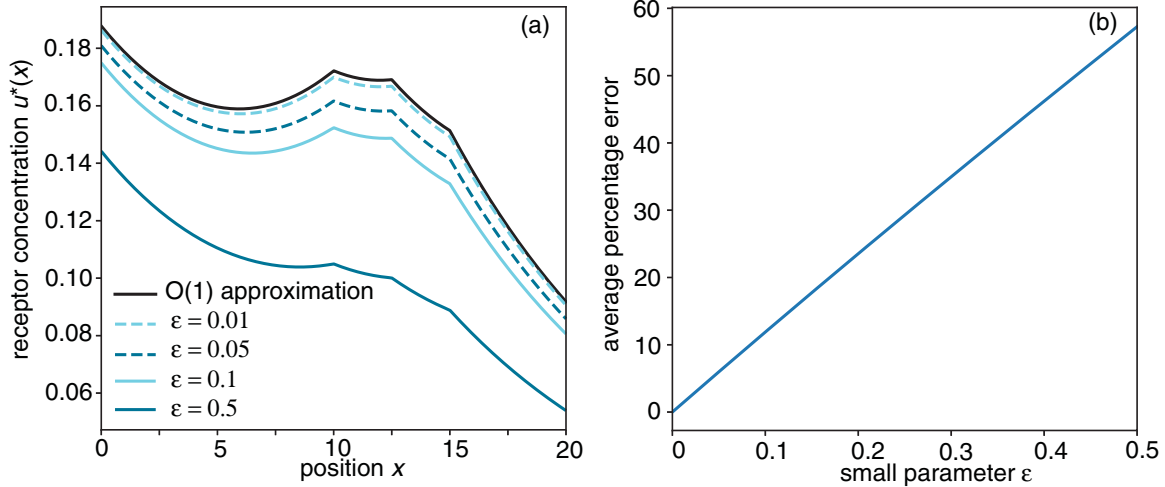
FIG. 2. (a) Plots of the steady-state receptor concentration for a dendrite with three synapses for various ϵ values with $\gamma_0 = 1$ and $\widehat{\gamma} = \epsilon\sqrt{\gamma D}$. The positions of the synapses are $x_k = x_0 + (k-1)\ell$, $k = 1, 2, 3$, where $x_0 = 10$ μm, $\ell = 2.5$ μm, and the other parameter values are as follows: $\sigma = 10^{-3}$ s^{-1}, $\gamma = 10^{-3}$ s^{-1}, $D = 0.1$ μm^2/s, $S_k = 10$, $\kappa_+ = 10^{-3}$ μm/s, $\kappa_- = 10^{-3}$ s^{-1}, and $J_0 = 10^{-3}$ s^{-1}. The solid black curve was calculated using the $O(1)$ approximation given in Eq. (3.12), and the dashed curves were calculated by numerically inverting the matrix equation (3.6) for u_k^* and substituting the result into Eq. (3.4). (b) Plot of the average percent error of the $O(1)$ approximation given by $\text{avg}_x|u_0^*(x) - \widehat{u}^*(x)|/\widehat{u}^*(x)$ as a function of ϵ, where $\widehat{u}^*$ is the steady-state numerical solution.

nonspatial compartmental model [23]. On the other hand, as synapses within a cluster become more separated, the multiplicative scaling rule breaks down. The multiplicative scaling of the synaptic strengths also breaks down when the effect of the somatic receptor flux becomes sufficiently strong. This can be achieved by either moving a synapse cluster closer to $x = 0$ or by increasing J_0, as illustrated in Fig. 3. We also see that when the somatic flux dominates, the steady-state solution becomes a monotonic decreasing function of x characterized by the $J_0 G(x, 0)$ term in Eq. (3.12), but when endocytosis dominates, local maxima occur in the neighborhoods of each of the two synapses. Hence, the steady-state concentration cannot detect the presence of synapses in the presence of a large flux and slow endocytosis rates.

Another observation is that if $\sigma > 0$, then the strengths of the synapses in a cluster are highly dependent on the number

of synapses in the cluster. Figure 4 shows that the synaptic strength significantly increases with the number of synapses in a cluster even if that cluster is moved farther from the receptor flux at $x = 0$. Again we see exponential decay in regions far from the synaptic clusters since the local receptor pools are governed by the somatic flux. In the neighborhood of the $N = 1$ cluster, the steady-state solution becomes an increasing function until the region near the $N = 6$ cluster is reached due to large increases in the size of the local receptor pool from perisynaptic endocytosis. The concentrations begin to decrease again as one moves from the $N = 6$ cluster to the $N = 12$ cluster despite the presence of a large number of synapses since the somatic receptor source sufficiently degrades in this region.

Finally, in Fig. 5 we show results from numerically simulating the full model (2.1) for a cluster of three synapses
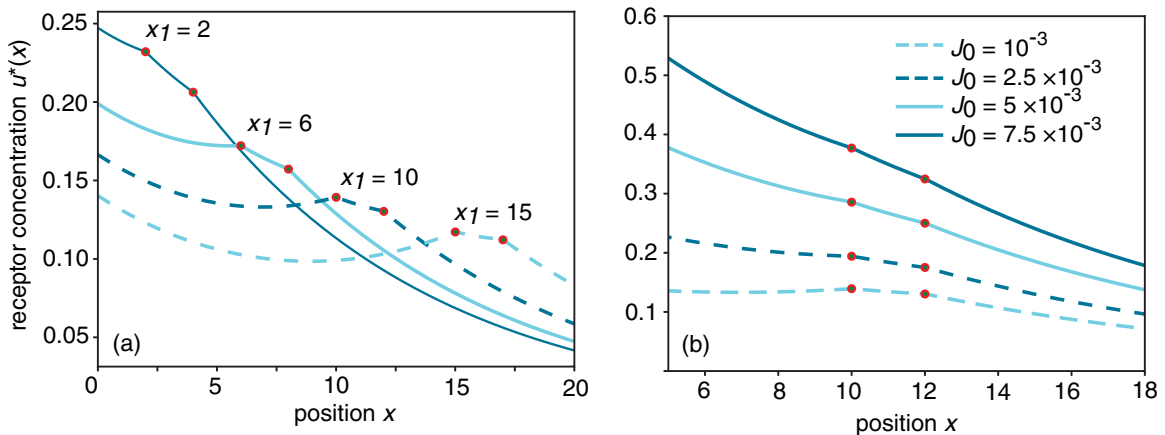

FIG. 3. Steady-state receptor concentration $u^*(x)$ per unit length for a pair of synapses separated by a fixed distance $\ell = 2$ μm. Other parameter values are as in Fig. 2. The concentration $u^*(x)$ is obtained by numerically inverting the matrix equation (3.6) for u_k^* and substituting the result into Eq. (3.4). (a) Plots of $u^*(x)$ as a function of x for different spatial locations of the synaptic pair and fixed ℓ. (b) Corresponding plots for different flux values J_0 and fixed synaptic locations $x_1 = 10$ μm, $x_2 = 12$ μm.
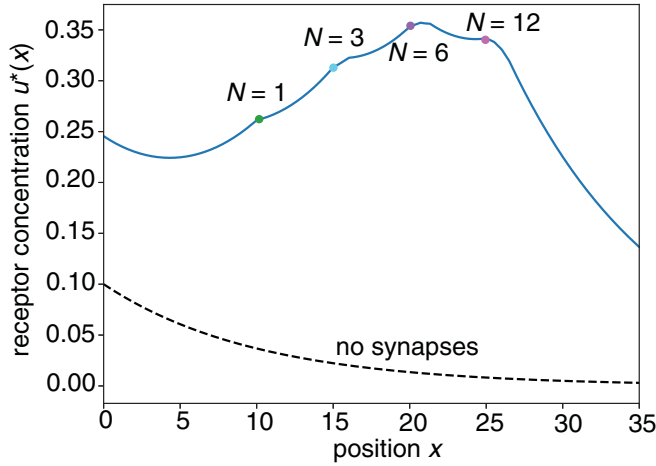
FIG. 4. Plot of the steady-state concentration $u^*(x)$ per unit length (obtained along lines identical to Fig. 3) in the case of four synaptic clusters at $x = 10 \, \mu$m, $x = 15 \, \mu$m, $x = 20 \, \mu$m, and $x = 25 \, \mu$m. Here $\sigma = 0.01 \, \text{s}^{-1}$, and other parameters are as in Fig. 2. The synapses in each cluster are distributed over a domain of size $\ell = 2 \, \mu$m, and the number of synapses in each cluster is varied. The dashed curve corresponds to the $O(1)$ bulk concentration when $\sigma = 0$, which is the same as when there are no synapses.

with nearest-neighbor distance ℓ. It can be seen that the fraction of bound receptors $r_k(t)$, $k = 1, 2, 3$, converges to a steady state r_k^* as $t \to \infty$. For sufficiently small ℓ the time-dependent curves $r_k(t)$ are approximately independent of k, and Eq. (3.14) provides a good approximation of the steady-state value. However, as the separation between the synapses increases, these curves asymptote to different steady-state values that are all lower than the original steady state. Therefore, tightly clustering the synapses has the effect of both homogenizing and increasing the steady-state synaptic strengths.

IV. LOCAL ACCUMULATION TIMES

Having obtained the steady-state solution, we can now calculate the accumulation times using Eqs. (2.6) and (2.7).
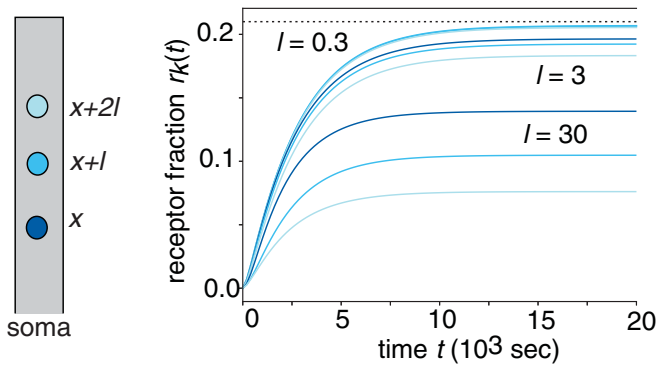

FIG. 5. Results of numerically simulating Eqs. (2.1) for a cluster of three identical synapses at positions $x_1 = x$, $x_2 = x + \ell$, and $x_3 = x + 2\ell$. Plots of $r_k(t)$, $k = 1, 2, 3$, for various synaptic spacings ℓ. The group of synapses starts at $x = 5 \, \mu$m. In the tightly clustered case ($\ell = 0.3 \, \mu$m), all three curves lie on top of each other, so only one is shown. The dashed horizontal line indicates the steady-state fraction $R = 0.21$. Other parameter values are as in Fig. 2.

In order to Laplace transform Eqs. (2.1), we will assume that concentration of receptors within a synapse is sufficiently small so that $\kappa_- \gg \kappa_+ u(x_k, t)$ and $r_k(t) \ll 1$. This means that nonlinear effects due to the saturation of the binding sites can be ignored. Laplace transforming Eqs. (2.1a)–(2.1c) using the initial conditions $u(x, 0) = 0$ and $r_j(0) = 0$ then gives

$$D \frac{\partial^2 \widetilde{u}(x, s)}{\partial x^2} - (s + \gamma) \widetilde{u}(x, s)$$
$$= - \sum_{j=1}^{N} \left(S_j [\kappa_- \widetilde{r}_j(s) - \kappa_+ \widetilde{u}(x_j, s)] \right.$$
$$\left. + \frac{\sigma}{s} - \widehat{\gamma} \widetilde{u}(x_j, s) \right) \delta(x - x_j),$$
(4.1a)

$$\widetilde{r}_k(s) = \frac{\kappa_+}{\kappa_- + s} \widetilde{u}(x_k, s).$$
(4.1b)

In analogy to Eq. (3.2), we introduce the s-dependent Neumann Green's function on $[0, \infty)$ according to

$$D \frac{\partial^2 G(x, y; s)}{\partial x^2} - (s + \gamma) G(x, y; s) = -\delta(x - y),$$
$$\left. \frac{\partial G(x, y; s)}{\partial x} \right|_{x=0} = 0.$$
(4.2)

From Eq. (3.3) we have

$$G(x, y; s) = \frac{1}{2\sqrt{D[s + \gamma]}} [e^{-\sqrt{(s+\gamma)/D}|x-y|} + e^{-\sqrt{(s+\gamma)/D}(x+y)}].$$
(4.3)

It then follows that

$$\widetilde{u}(x, s) = \frac{J_0}{s} G(x, 0; s)$$
$$+ \sum_{k=1}^{N} \left(\frac{\sigma}{s} - \left[\frac{s S_k \kappa_+}{\kappa_- + s} + \widehat{\gamma} \right] \widetilde{u}(x_k, s) \right) G(x, x_k; s).$$
(4.4)

Multiplying this equation by s and taking the limit $s \to 0$ immediately recovers the steady-state solution (3.4) since $G(x, x_k, 0) = G(x, x_k)$.

It remains to determine the synaptic terms $\widetilde{u}(x_j, s)$. Setting $x = x_j$ in Eq. (4.4) gives the matrix equations

$$\widetilde{u}(x_j, s) = \frac{J_0}{s} G(x_j, 0, s)$$
$$+ \sum_{k=1}^{N} \left(\frac{\sigma}{s} - \left[\frac{s S_k \kappa_+}{\kappa_- + s} + \widehat{\gamma} \right] \widetilde{u}(x_k, s) \right) G(x_j, x_k, s).$$
(4.5)

This can be rewritten as the matrix equation

$$\sum_{k=1}^{N} \left(\delta_{j,k} + \left[s\Gamma(s) S_k + \frac{\widehat{\gamma}}{\sqrt{[s + \gamma]D}} \right] \mathcal{G}_{jk}(s) \right) \widetilde{u}(x_k, s) = \frac{H_j(s)}{s},$$
(4.6)

with

$$\mathcal{G}_{jk}(s) = \sqrt{[s+\gamma]D} G(x_j, x_k, s), \tag{4.7a}$$

$$H_j(s) = J_0 G(x_j, 0, s) + \sigma \sum_{k=1}^{N} G(x_j, x_k, s), \tag{4.7b}$$

$$\Gamma(s) = \frac{\kappa_+}{\kappa_- + s} \frac{1}{\sqrt{[s+\gamma]D}}. \tag{4.7c}$$

Note that $H_j(0) = u_0^*(x_j)$, with $u_0^*(x)$ defined by Eq. (3.12). Again we will invert the matrix by exploiting the relatively slow rate of endocytosis. Since we are ultimately interested in the limit $s \to 0$, we will also assume that s is small and impose the inequalities (3.7) with $s = O(\epsilon)$. We can now carry out a perturbation expansion of Eq. (4.6) with respect to ϵ by writing

$$\{\mathbf{I} + \mathcal{G}(s)[s\Gamma(s)\mathbf{S} + \epsilon\gamma_0\mathbf{I}]\}^{-1}$$
$$= \mathbf{I} - \mathcal{G}(s)[s\Gamma(s)\mathbf{S} + \epsilon\gamma_0\mathbf{I}] + \cdots, \tag{4.8}$$

with $\mathbf{S} = \mathrm{diag}(S_1, S_2, \ldots, S_N)$, and introduce the series expansion

$$\tilde{u}(x_k, s) = \tilde{u}_0(x_k, s) + \epsilon\tilde{u}_1(x_k, s) + \epsilon^2\tilde{u}_2(x_k, s) + \cdots. \tag{4.9}$$

Substituting into Eq. (4.5) gives

$$\tilde{u}_0(x_j, s) + \epsilon\tilde{u}_1(x_j, s) + \cdots$$
$$= \frac{1}{s} \sum_{k=1}^{N} \{\delta_{j,k} - \mathcal{G}_{jk}(s)[s\Gamma(s)S_k + \epsilon\gamma_0] + \cdots\} H_k(s). \tag{4.10}$$

We thus obtain the leading order solution

$$\tilde{u}_0(x_j, s) = \frac{1}{s} \left[H_j(s) - s\Gamma(s) \sum_{k=1}^{N} \mathcal{G}_{jk}(s) S_k H_k(s) \right]. \tag{4.11}$$

Having obtained a series expansion of $\tilde{u}(x_j, s)$, we have a corresponding series expansion of the fraction of bound receptors according to Eq. (4.1c):

$$\tilde{r}_j(s) = \tilde{r}_{j,0}(s) + \epsilon\tilde{r}_{j,1}(s) + \cdots, \tag{4.12}$$

$$\tilde{r}_{j,n}(s) = \frac{\kappa_+}{\kappa_- + s} \tilde{u}_n(x_j, s). \tag{4.13}$$

Substituting Eqs. (4.11)–(4.13) into Eq. (2.7) yields

$$\tau_j = -\frac{1}{r_j^*} \frac{d}{ds} \left[\frac{s\kappa_+}{\kappa_- + s} [\tilde{u}_0(x_j, s) + \epsilon\tilde{u}_1(x_j, s) + \cdots] \right]\Bigg|_{s=0} = -\frac{1}{r_{j,0}^*} \frac{d}{ds} \left[\frac{\kappa_+}{\kappa_- + s} \left(H_j(s) - s\Gamma(s) \sum_{k=1}^{N} \mathcal{G}_{jk}(s) H_k(s) + \cdots \right) \right]\Bigg|_{s=0}$$

$$= -\frac{1}{r_{j,0}^*} \frac{\kappa_+}{\kappa_-} \left[\partial_s H_j(0) - \frac{1}{\kappa_-} H_j(0) - \Gamma(0) \sum_{k=1}^{N} \mathcal{G}_{jk}(0) S_k H_k(0) \right] + O(\epsilon). \tag{4.14}$$

In the unsaturated regime,

$$r_{j,0}^* = \frac{\kappa_+ H_j(0)}{\kappa_-}. \tag{4.15}$$

Hence, to leading order, we have

$$\tau_j = \frac{|\partial_s H_j(0)|}{H_j(0)} + \frac{\kappa_+}{\kappa_-} \sum_{k=1}^{N} S_k \frac{H_k(0)}{H_j(0)} G(x_j, x_k) + \frac{1}{\kappa_-}. \tag{4.16}$$

In the limit $\sigma \to 0$, we obtain the simplified expression

$$\tau_j = T_0(x_j) + \frac{\kappa_+}{\kappa_-} \sum_{k=1}^{N} S_k \frac{G(x_k, 0)}{G(x_j, 0)} G(x_j, x_k) + \frac{1}{\kappa_-}, \tag{4.17}$$

where

$$T_0(x) = \frac{1}{2} \left[\frac{1}{\gamma} + \frac{x}{\sqrt{D\gamma}} \right] \tag{4.18}$$

is the accumulation time for pure diffusion and endocytosis (or degradation) [30–32], that is, in the absence of any synapses. This corresponds to dropping the second line of Eq. (2.1a). Note that since the accumulation time is defined in terms of the difference of the current concentration from the steady-state concentration, it is independent of the somatic

flux J_0 when $\sigma = 0$. We have used the result

$$\partial_s G(x, y; s)$$
$$= -\frac{1}{4\sqrt{D[s+\gamma]}} \left[\frac{1}{\gamma+s} + \frac{|x-y|}{\sqrt{D[\gamma+s]}} \right] e^{-|x-y|\sqrt{(s+\gamma)/D}}$$
$$- \frac{1}{4\sqrt{D[s+\gamma]}} \left[\frac{1}{\gamma+s} + \frac{x+y}{\sqrt{D[\gamma+s]}} \right] e^{-(x+y)\sqrt{(s+\gamma)/D}},$$

which implies

$$\partial_s G(x, 0; s)$$
$$= -\frac{1}{2\sqrt{D[s+\gamma]}} \left[\frac{1}{\gamma+s} + \frac{x}{\sqrt{D[\gamma+s]}} \right] e^{-x\sqrt{(s+\gamma)/D}}.$$

Substituting Eqs. (4.4) and (4.11) into Eq. (2.6) yields the following equation for the accumulation time in the bulk:

$$T(x) = \frac{J_0|\partial_s G(x, 0; 0)|}{u_0^*(x)} + \frac{\kappa_+}{\kappa_-} \sum_{k=1}^{N} S_k \frac{u_0^*(x_k)}{u_0^*(x)} G(x, x_k) + O(\epsilon). \tag{4.19}$$

In the limit that $\sigma \to 0$, we obtain

$$T(x) = T_0(x) + \frac{\kappa_+}{\kappa_-} \sum_{k=1}^{N} S_k \frac{G(x_k, 0)}{G(x, 0)} G(x, x_k) + O(\epsilon). \tag{4.20}$$
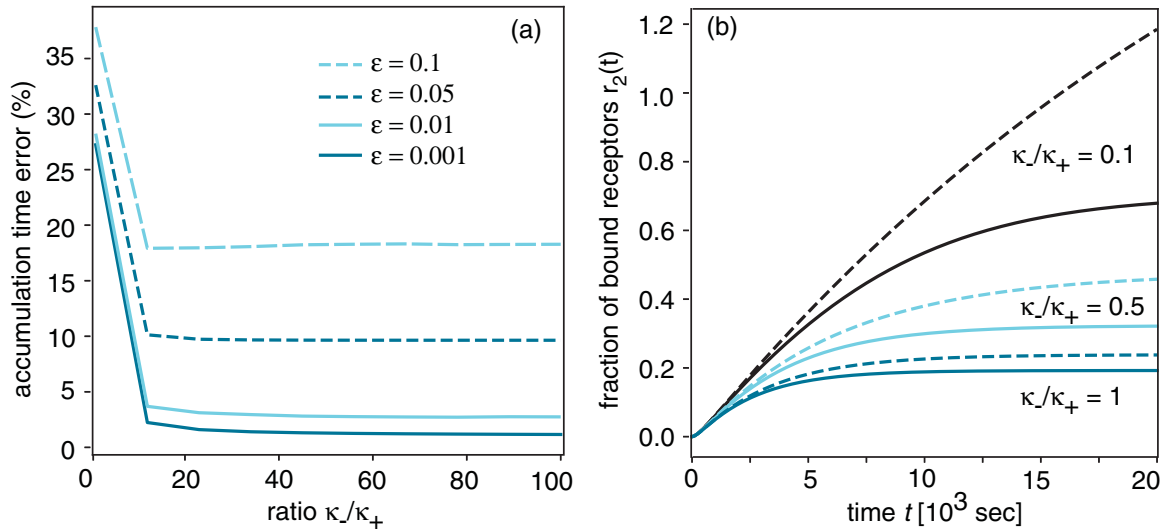
FIG. 6. (a) Plots of the percentage error E of the $O(1)$ synaptic accumulation times τ_k with respect to the numerical accumulation times $\widehat{\tau}_k$ with $E = \frac{1}{N}\sum_{k=1}^{N}|\tau_k - \widehat{\tau}_k|/\widehat{\tau}_k$. The numerical accumulation times are obtained by simulating Eq. (2.1) to determine $r_k(t)$ and computing r_k^* using Eq. (3.4) and numerically solving Eq. (3.6). $\widehat{\tau}_k$ is then calculated by numerically integrating $z_k(t) = 1 - r_k(t)/r_k^*$. The synapses are located at $x_k = x_0 + (k-1)\ell$, where $x_0 = 5\ \mu$m and $\ell = 0.1\ \mu$m. We fix $\kappa_+ = 10^{-3}\ \mu$m/s and vary the ratio κ_-/κ_+. The other parameters are as in Fig. 2. (b) Plots of the fraction of bound slot proteins for the second synapse in the cluster generated by numerically simulating Eq. (2.1) (solid curves) and the linearized version of Eq. (2.1) (dashed curves).

In Fig. 6(a), we plot the percentage error of Eq. (4.16) with respect to the numerical synaptic accumulation times calculated using simulations in Eq. (2.1). We see that the error decreases linearly until $\kappa_-/\kappa_+ \approx 12.5$. The error is approximately constant after this point, indicating that the assumption that the slot proteins are not saturated is a reasonable approximation. This can also be seen in Fig. 6(b), where we plot the trajectories of the fraction of bound slot proteins for both Eq. (2.1) and the linearized version of Eq. (2.1). We see that the linearized model provides an accurate approximation of the full model when $\kappa_-/\kappa_+ \geqslant 1$. Furthermore, for $\epsilon \leqslant 0.01$ and $\kappa_-/\kappa_- > 10$, the $O(1)$ approximation of the accumulation times is within 10% of the numerical results. Finally, we see that for $\kappa_-/\kappa_+ = 0.1$ the breakdown of the linear approximation yields bound receptor fractions that exceed unity.

Comparing Eqs. (4.16) and (4.17) with the steady-state solution (3.11) establishes a number of significant differences. First, in the limit $\sigma \to 0$ (no exocytosis), the $O(1)$ steady-state receptor concentration is purely local, $u_{j,0}^* = J_0 G(x_j, 0)$. This means that the presence of a set of synapses does not affect the $O(1)$ bulk concentration $u_0^*(x)$. Hence, the fraction of bound receptors in a given synapse is independent of the other synapses. On the other hand, synaptic interactions have an $O(1)$ effect on the local accumulation time τ_j, even when $\sigma = 0$. Second, this $O(1)$ contribution depends on the number of slot proteins S_k, $k = 1, \ldots, N$, in all the synapses. These features are illustrated in Fig. 7, where we plot the accumulation times τ_j, $j = 1, 2$, for a pair of synapses with x_1 fixed and $x_2 = x_1 + \ell$ for a variable spacing ℓ. The dependence of τ_j on ℓ and S_2 can be seen even when $\sigma = 0$. The accumulation
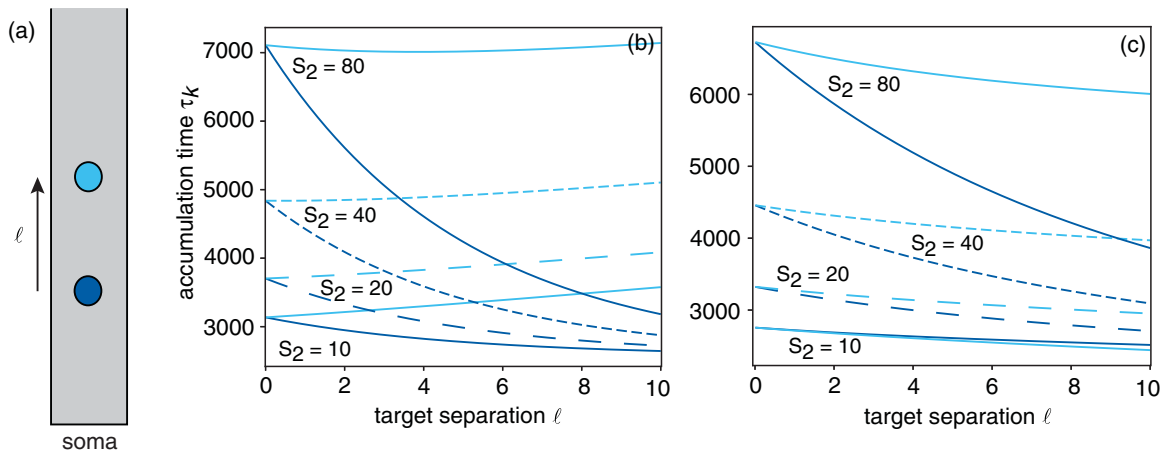

FIG. 7. (a) Pair of synapses with $x_1 = 10\ \mu$m and $x_2 = x_1 + \ell$. (b) Plot of the accumulation times τ_1 (dark curves) and τ_2 (light curves) as a function of the separation ℓ for $\sigma = 0$, $S_1 = 10$, and various values of the slot protein number S_2: $S_2 = 10, 20, 40, 80$. (c) Corresponding plots for $\sigma = 0.1$. The other parameter values are as in Fig. 2. The accumulation times $\tau_{1,2}$ are calculated using Eq. (4.16).
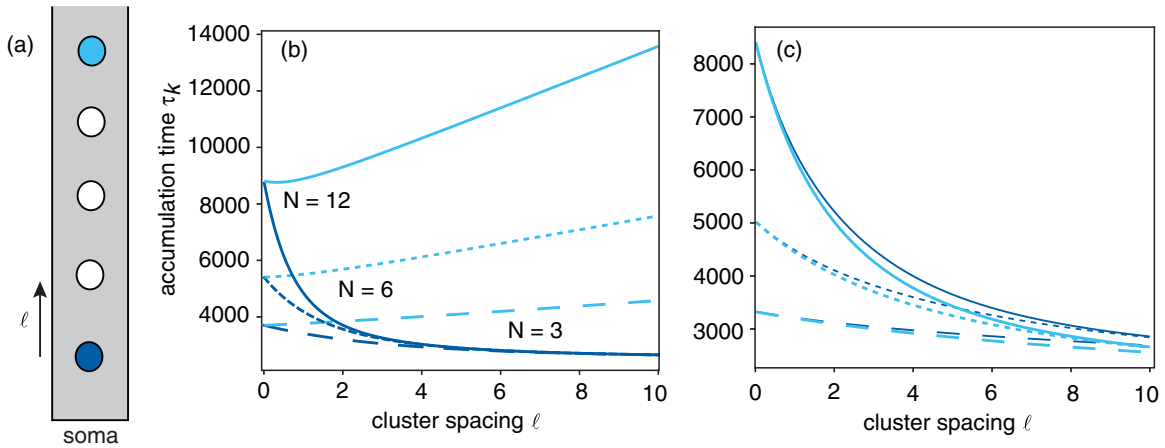
FIG. 8. (a) Cluster of N synapses at spatial locations $x_k = x_1 + (k-1)\ell$, where $x_1 = 10$ μm. (b) Plots of the accumulation times τ_1 and τ_N, respectively, for the first and last synapses in the cluster as a function of the cluster spacing ℓ and various cluster sizes $N = 3, 6, 12$ for $\sigma = 0$. (c) Corresponding plots for $\sigma = 0.1$. The other parameter values are as in Fig. 2. The accumulation times $\tau_{1,N}$ are calculated using Eq. (4.16).

time τ_2 has a weaker dependence on ℓ than τ_1, while the difference $\tau_2 - \tau_1$ for fixed ℓ is reduced as σ increases from zero. In Fig. 8 we show analogous plots for τ_1 and τ_N in a cluster of N synapses with variable spacing ℓ. It can be seen that adding synapses to a highly separated cluster does not affect the value of τ_1 but increases τ_N significantly due to the other synapses inhibiting access to the receptor pool. In the case of a tight cluster of synapses, the accumulation time is approximately the same for each synapse in the cluster. As the spacing ℓ is increased, the synapses located closer to $x = 0$ reach steady state more rapidly while the accumulation times of the synapses on the right end of the domain do not change significantly [see Fig. 9(a)]. On the other hand, if $\sigma \geqslant J_0$ and $S_i = S$ for all j, then the homogeneity of the synaptic accumulation times is preserved even when the synapses have a large separation. We also observe that the accumulation times are reduced significantly for all synapses in the cluster [see Fig. 9(b)].

$O(1)$ synaptic interactions also appear in the bulk accumulation time $T(x)$. This is illustrated in Fig. 10, where we show example plots of $T(x)$ as a function of dendritic location x.

We assume that there are several synaptic clusters of different sizes. In the absence of any synapses, the corresponding accumulation time $T_0(x)$ increases linearly with x. On the other hand, the presence of synaptic clusters significantly increases $T(x)$, which now varies nonlinearly with x. If $\sigma \ll J_0$, then $T(x)$ is a monotonically increasing function of x, with $T'(x)$ having a local maximum in a neighborhood of each cluster [see Fig. 10(a)]. If $\sigma \geqslant J_0$, then $T(x)$ is no longer monotonic and shows a much weaker dependence on x, as demonstrated in Fig. 10(b). These two distinct modes of behavior seem to arise from the relative dominance of the two sources of receptors. When the local pool of receptors available to a cluster is dominated by exocytosis, the accumulation time becomes homogeneous and is mostly a function of the total number of synapses in each cluster. When the local pool of receptors is dominated by the somatic flux at $x = 0$, the heterogeneity of the accumulation times increases, and they become mostly a function of their position relative to $x = 0$.

Finally, the transient heterosynaptic effects of the number of slot proteins S_k, $k = 1, \ldots, N$, across a cluster of synapses is illustrated in Fig. 11. We see that the steady-state values
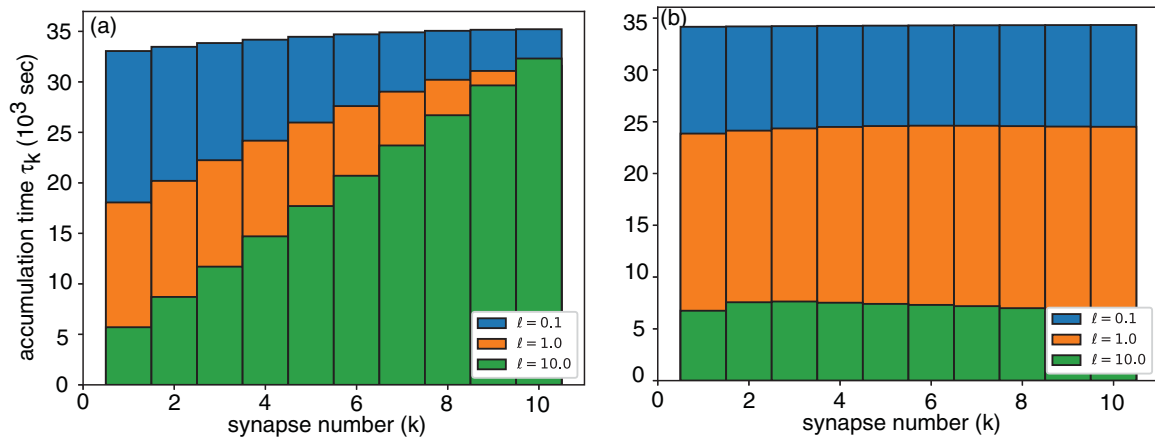

FIG. 9. Dependence on synaptic spacing ℓ for a cluster of $N = 10$ identical synapses with $S_k = 50$. (a) Plots of the accumulation times τ_k given by Eq. (4.17) in the case with $\sigma = 0$. The synapses are located at the positions $x_k = x_1 + (k-1)\ell$ with $x_1 = 10$ μm and ℓ varied. (b) Corresponding plots for $\sigma = 10^{-3}$. The other parameter values are as in Fig. 2.
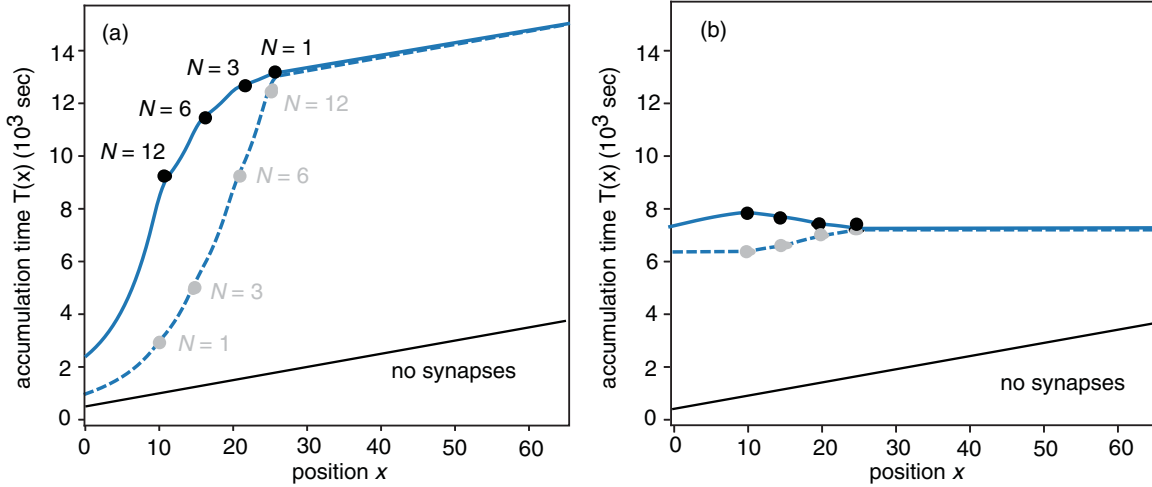
FIG. 10. (a) Plots of the bulk accumulation time $T(x)$ given by Eq. (4.20) for $\sigma = 0$ in the case of four synaptic clusters at $x = 10$ μm, $x = 15$ μm, $x = 20$ μm, and $x = 25$ μm. The synapses in each cluster are distributed over a domain of size $\ell = 2$ μm, and the number of synapses in each cluster is varied. (The dashed lines represent the results when the order of the cluster sizes is reversed.) (b) Corresponding plots for $\sigma = 0.1$. Other parameter values are as in Fig. 2.

of the fractions of bound slot proteins is independent of S_k but the total time to steady state increases with S_k. This is consistent with the accumulation time calculations. Furthermore, increasing the number of slot proteins in a subset of the synapses in a cluster before the steady-state value is reached has the effect of increasing the time to steady state for all the synapses in the cluster, including the unaltered synapses. This implies that the total number of slot proteins in a cluster is the important parameter that controls the dynamics of a synapse rather than the number of slot proteins in an individual synapse.

V. DISCUSSION

In this paper, we used a diffusion-trapping model of dendritic receptor trafficking to investigate the effects of spatial heterogeneity on the steady-state distribution of synaptic weights and the relaxation to steady state. The model took

the form of a set of RD equations, in which the dendrite was represented as a semi-infinite cable and each synapse was taken to be a point source. The latter leveraged the nonsingular behavior of one-dimensional Green's functions. We first derived a solution to the associated steady-state equations, which took the form of a perturbation series expansion in the small dimensionless parameter ϵ that characterized the relatively slow rates of endocytosis. We showed that for a cluster of closely spaced synapses, the steady-state fraction of bound receptors in each synapse is the same to leading order (multiplicative scaling). However, it was found that the synaptic strengths are coupled at $O(\epsilon)$, and a breakdown of multiplicative scaling can be observed by increasing the size of the synaptic domain or by increasing the strength of the source of receptors from the soma. The latter was achieved by both moving the cluster closer to $x = 0$ and increasing the receptor flux. Additionally, we observed that the strengths of all synapses in a cluster can be increased by reducing the size
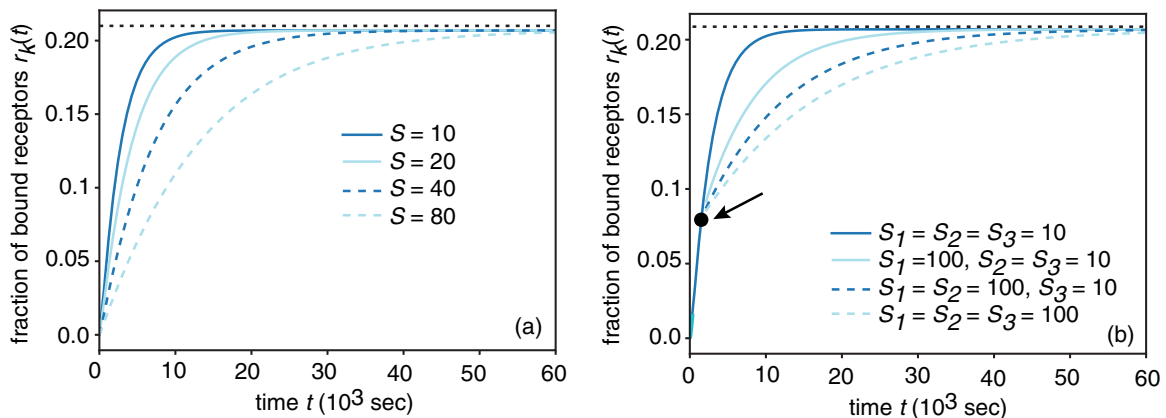

FIG. 11. Transient heterosynaptic effects in a cluster of three synapses located at $x_k = x + (k-1)\ell$ with $x = 5$ μm and $\ell = 0.1$ μm. (a) Plots of the fraction of bound receptors $r_k(t)$ for $S_k = S$, $k = 1, 2, 3$, and various values of S. (b) Corresponding plots when the number of slot proteins in one or more of the synapses is increased to $S_k = 100$ at $t = 1500$ s (as indicated by the arrow). The other parameter values are as in Fig. 2. The dashed horizontal lines indicate the steady-state fraction $R = 0.21$ as in Fig. 5. Results are obtained by numerically simulating the full equations (2.1).

of the synaptic domain or increasing the number of synapses in the cluster.

In order to study the temporal dynamics of the receptor trafficking process, we calculated a set of local accumulation times. In contrast to spectral methods, which provide a global measure of the rate at which the system reaches steady state, the accumulation times determine how rapidly steady state is approached at each point in the bulk and at each synapse. The accumulation times were calculated by solving the linearized RD equations in Laplace space using Green's function methods analogous to those used to obtain the steady-state solution. Contrary to the results obtained from the steady-state analysis, we found that the accumulation times had a strong dependence on the number of slot proteins in the synapses at order $O(1)$. We thus observed that dynamically altering the number of slot proteins in a single synapse or subset of synapses within a cluster altered the trajectories to steady state as a whole rather than altering the trajectories of only the modified synapses. This implies that the total number of slot proteins in a cluster is the important parameter for controlling the dynamics of the trajectories rather than the distribution of slot proteins among the individual synapses within a cluster.

Interestingly, two distinct modes of behavior were observed, depending on whether exocytosis or the somatic flux was the dominant source of receptors, which can be seen in Figs. 7 and 8. The $O(1)$ dependence on the spatial distribution of synapses within a cluster was similar to the steady-state results when $\sigma > 0$, but this dependence could be eliminated such that the synaptic accumulation times were homogeneous even for large synaptic separations by letting $\sigma \to 0$. Fur-

thermore, when σ was sufficiently large, not only did the presence of a cluster of synapses cause a significant increase in accumulation times of the points near the cluster, but this increase was communicated to all points to the right of the cluster as well.

One natural extension of the current model is to consider diffusion in a 2D cellular membrane, rather than a 1D dendritic cable in which the synapses are represented as point sources or sinks at locations x_k on the cable. The latter exploits the quasi-1D geometry of a dendrite over length scales of the order of hundreds of microns. However, the quasi-1D approximation is not appropriate for synapses distributed over a more local region of a dendrite or for synapses located in the somatic membrane. In such cases one has to take Ω to be a 2D domain. Moreover, one can no longer treat the synapses as point-like since the corresponding 2D Green's function has a logarithmic singularity. However, if the synapses are relatively small compared to the size of the domain, then one can use asymptotic perturbation methods along the lines of [37]. Finally, in future work it would be interesting to explore how the relaxation times analyzed in this paper overlap with typical spike timing-dependent plasticity experiments. The latter stimulate synapses using a pair or triplet of excitation pulses, and the resulting synaptic modifications can depend on the order of presynaptic and postsynaptic spiking within a critical window of tens of milliseconds; see the review in [45]. Although this is several orders of magnitude faster than the accumulation times for receptor trafficking, there could be an interplay between the latter and the timescales associated with sequences of synaptic modifications.

[1] J. Meier, C. Vannier, A. Serge, A. Triller, and D. Choquet, Fast and reversible trapping of surface glycine receptors by gephyrin, Nat. Neurosci. **4**, 253 (2001).

[2] A. J. Borgdorff and D. Choquet, Regulation of AMPA receptor lateral movements, Nature (London) **417**, 649 (2002).

[3] M. Dahan, S. Levi, C. Luccardini, P. Rostaing, B. Riveau and A. Triller, Diffusion dynamics of glycine receptors revealed by single-quantum dot tracking, Science **302**, 442 (2003).

[4] D. S. Bredt and R. A. Nicoll, AMPA receptor trafficking at excitatory synapses, Neuron **40**, 361 (2003).

[5] D. Choquet and A. Triller, The role of receptor diffusion in the organization of the postsynaptic membrane, Nat. Rev. Neurosci. **4**, 251 (2003).

[6] L. Groc, M. Heine, L. Cognet, K. Brickley, F. A. Stephenson, B. Lounis, and D. Choquet, Differential activity-dependent regulation of the lateral mobilities of AMPA and NMDA receptors, Nat. Neurosci. **7**, 695 (2004).

[7] G. L. Collinridge, J. T. R. Isaac, and Y. T. Wang, Receptor trafficking and synaptic plasticity, Nat. Rev. Neurosci. **5**, 952 (2004).

[8] A. Triller and D. Choquet, Surface trafficking of receptors between synaptic and extrasynaptic membranes: And yet they do move!, Trends Neurosci. **28**, 133 (2005).

[9] M. C. Ashby, S. R. Maier, A. Nishimune, and J. M. Henley, Lateral diffusion drives constitutive exchange of AMPA receptors at dendritic spines and is regulated by spine morphology, J. Neurosci. **26**, 7046 (2006).

[10] M. D. Ehlers, M. Heine, L. Groc, M.-C. Lee, and D. Choquet, Diffusional trapping of GluR1 AMPA receptors by input-specific synaptic activity, Neuron **54**, 447 (2007).

[11] K. Gerrow and A. Triller, Synaptic stability and plasticity in a floating world, Curr. Opin. Neurobiol. **20**, 631 (2010).

[12] J. M. Henley, E. A. Barker, and O. O. Glebov, Routes, destinations and delays: Recent advances in AMPA receptor trafficking, Trends Neurosci. **34**, 258 (2011).

[13] D. Choquet and A. Triller, The dynamic synapse, Neuron **80**, 691 (2013).

[14] R. H. Roth, Y. Zhang, and R. L. Huganir, Dynamic imaging of AMPA receptor trafficking in vitro and in vivo, Curr. Opin. Neurobiol. **45**, 51 (2017).

[15] D. Choquet, Linking nanoscale dynamics of AMPA receptor organization to plasticity of excitatory synapses and learning, J. Neurosci. **38**, 9318 (2018).

[16] S. A. Maynard and A. Triller, Inhibitory receptor diffusion dynamics, Front. Mol. Neurosci. **12**, 313 (2019).

[17] M. D. Ehlers, Reinsertion or degradation of AMPA receptors determined by activity-dependent endocytic sorting, Neuron **28**, 511 (2000).

[18] B. A. Earnshaw and P. C. Bressloff, A biophysical model of AMPA receptor trafficking and its regulation during LTP/LTD, J. Neurosci. **26**, 12362 (2006).

[19] D. Holcman and A. Triller, Modeling synaptic dynamics driven by receptor lateral diffusion, Biophys. J. **91**, 2405 (2006).

[20] P. C. Bressloff and B. A. Earnshaw, Diffusion-trapping model of receptor trafficking in dendrites, Phys. Rev. E **75**, 041915 (2007).

[21] B. A. Earnshaw and P. C. Bressloff, Modeling the role of lateral membrane diffusion on AMPA receptor trafficking along a spiny dendrite, J. Comput. Neurosci. **25**, 366 (2008).

[22] K. Czöndör, M. Mondina, M. Garciaa, M. Heinec, R. Frischknechtc, D. Choquet, J. B. Sibaritaa, and O. R. Thoumine, A unified quantitative model of AMPA receptor trafficking at synapses, Proc. Natl. Acad. Sci. USA **109**, 3522 (2012).

[23] J. Triesch, A. D. Vo, and A. S. Hafner, Competition for synaptic building blocks shapes synaptic plasticity, eLIFE **7**, e37836 (2018).

[24] C. Salvatico, C. G. Specht, and A. Triller, Synaptic receptor dynamics: From theoretical concepts to deep quantification and chemistry in cellulo, Neuropharmacology **88**, 2 (2015).

[25] K. Sekimoto and A. Triller, Compatibility between itinerant synaptic receptors and stable postsynaptic structure, Phys. Rev. E **79**, 031905 (2009).

[26] C. A. Haselwandter, M. Calamai, M. Kardar, A. Triller, and R. A. da Silveira, Formation and Stability of Synaptic Receptor Domains, Phys. Rev. Lett. **106**, 238104 (2011).

[27] C. A. Haselwandter, M. Calamai, M. Kardar, A. Triller, and R. A. da Silveira, Self-assembly and plasticity of synaptic domains through a reaction-diffusion mechanism, Phys. Rev. E **92**, 032705 (2015).

[28] V. Hakim and J. Ranft, Lifetime of a structure evolving by cluster aggregation and particle loss, and application to postsynaptic scaffold domains, Phys. Rev. E **101**, 012411 (2020).

[29] T. Chapdelaine, V. Hakim, A. Triller, J. Ranft, and C. G. Specht, Reciprocal stabilization of glycine receptors and gephyrin scaffold proteins at inhibitory synapses, Biophys. J. **120**, 805 (2021).

[30] A. M. Berezhkovskii, C. Sample, and S. Y. Shvartsman, How long does it take to establish a morphogen gradient? Biophys. J. **99**, L59 (2010).

[31] A. M. Berezhkovskii, C. Sample, and S. Y. Shvartsman, Formation of morphogen gradients: Local accumulation time, Phys. Rev. E **83**, 051906 (2011).

[32] P. Gordon, C. Sample, A. M. Berezhkovskii, C. B. Muratov, and S. Y. Shvartsman, Local kinetics of morphogen gradients, Proc. Natl. Acad. Sci. USA **108**, 6157 (2011).

[33] P. C. Bressloff, S. D. Lawley, and P. Murphy, Protein concentration gradients and switching diffusions, Phys. Rev. E **99**, 032409 (2019).

[34] P. C. Bressloff, Accumulation time of stochastic processes with resetting, J. Phys. A **54**, 354001 (2021).

[35] P. C. Bressloff, Local accumulation time for diffusion in cells with gap junction coupling, Phys. Rev. E **105**, 034404 (2022).

[36] S. V. Ramanan and P. R. Brink, Exact solution of a model of diffusion in an infinite chain or monolayer of cells coupled by gap junctions, Biophys. J. **58**, 631 (1990).

[37] P. C. Bressloff, B. A. Earnshaw, and M. J. Ward, Diffusion of protein receptors on a cylindrical dendritic membrane with partially absorbing targets, SIAM J. Appl. Math. **68**, 1223 (2008).

[38] D. Holcman and Z. Schuss, Escape through a small opening: Receptor trafficking in a synaptic membrane, J. Stat. Phys. **117**, 975 (2004).

[39] A. Biess, E. Korkotian, and D. Holcman, Diffusion in a dendritic spine: The role of geometry, Phys. Rev. E **76**, 021922 (2007).

[40] C. M. Simon, I. Hepburn, W. Chen, and E. De Schutter, The role of dendritic spine morphology in the compartmentalization and delivery of surface receptors, J. Comput. Neurosci. **36**, 483 (2014).

[41] M. Adrian, R. Kusters, C. Storm, C. C. Hoogenraad, and L. C. Kapitein, Probing the interplay between dendritic spine morphology and membrane-bound diffusion, Biophys. J. **113**, 2261 (2017).

[42] H. D. MacGillavry, J. M. Kerr, and T. A. Blanpied, Lateral organization of the postsynaptic density, Mol. Cell. Neurosci. **48**, 321 (2011).

[43] D. Nair, E. Hosy, J. D. Petersen, A. Constals, G. Giannone, D. Choquet, and J. B. Sibarita, Super-resolution imaging reveals that AMPA receptors inside synapses are dynamically organized in nanodomains regulated by PSD95, J. Neurosci. **33**, 13204 (2013).

[44] J. M. Henley and K. A. Wilkinson, Synaptic AMPA receptor composition in development, plasticity and disease, Nat. Rev. Neurosci. **17**, 337 (2016).

[45] N. Caporale and Y. Dan, Spike timing-dependent plasticity: A Hebbian learning rule, Annu. Rev. Neurosci. **31**, 25 (2008).